



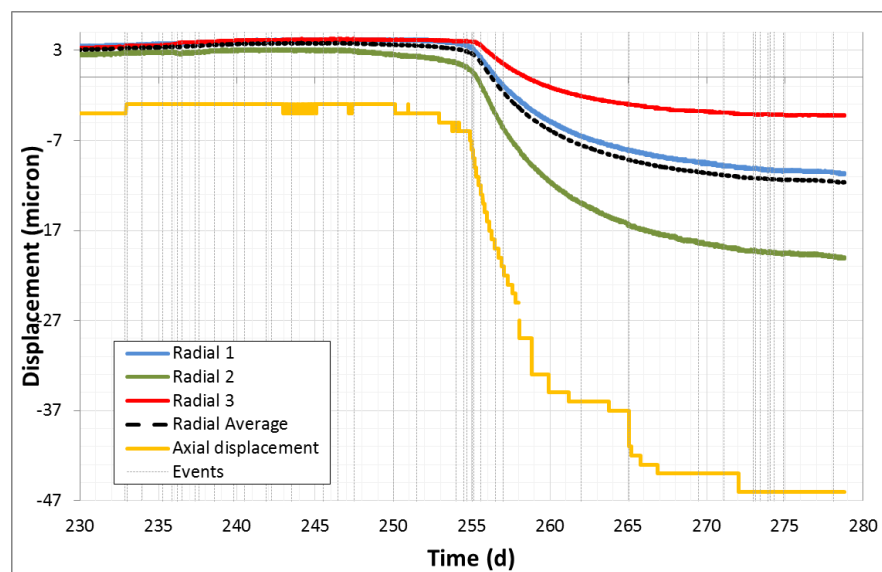
**British  
Geological Survey**

NATURAL ENVIRONMENT RESEARCH COUNCIL

# Update on dilatancy associated with onset of gas flow in Callovo-Oxfordian claystone; Progress report on test SPP\_COx-2

Minerals and Waste Programme

Commissioned Report CR/11/110





BRITISH GEOLOGICAL SURVEY

MINERALS AND WASTE PROGRAMME

COMMISSIONED REPORT CR/11/110

# Update on dilatancy associated with onset of gas flow in Callovo-Oxfordian claystone; Progress report on test SPP\_COx-2

R.J. Cuss and J.F. Harrington

*Keywords*

SPP, FORGE, stress path testing, Callovo-Oxfordian claystone, COx.

*Front cover*



Graph of strain observed in 3 radial directions and axially showing dilatancy at the onset of gas flow.


*Bibliographical reference*

CUSS, R.J. AND HARRINGTON, J.F. 2011. Update on dilatancy associated with onset of gas flow in Callovo-Oxfordian claystone; Progress report on test SPP\_COx-2. *British Geological Survey Commissioned Report*, CR/11/110. 34pp.

Copyright in materials derived from the British Geological Survey's work is owned by the Natural Environment Research Council (NERC) and/or the authority that commissioned the work. You may not copy or adapt this publication without first obtaining permission. Contact the BGS Intellectual Property Rights Section, British Geological Survey, Keyworth, e-mail [ipr@bgs.ac.uk](mailto:ipr@bgs.ac.uk). You may quote extracts of a reasonable length without prior permission, provided a full acknowledgement is given of the source of the extract.

© NERC 2011. All rights reserved

Reviewed by:    
RJ Cuss JF Harrington

Approved by:   
RP Shaw

Keyworth, Nottingham British Geological Survey 2011

## BRITISH GEOLOGICAL SURVEY

The full range of our publications is available from BGS shops at Nottingham, Edinburgh, London and Cardiff (Welsh publications only) see contact details below or shop online at [www.geologyshop.com](http://www.geologyshop.com)

The London Information Office also maintains a reference collection of BGS publications, including maps, for consultation.

We publish an annual catalogue of our maps and other publications; this catalogue is available online or from any of the BGS shops.

*The British Geological Survey carries out the geological survey of Great Britain and Northern Ireland (the latter as an agency service for the government of Northern Ireland), and of the surrounding continental shelf, as well as basic research projects. It also undertakes programmes of technical aid in geology in developing countries.*

*The British Geological Survey is a component body of the Natural Environment Research Council.*

*British Geological Survey offices*

### **BGS Central Enquiries Desk**

Tel 0115 936 3143 Fax 0115 936 3276  
email [enquires@bgs.ac.uk](mailto:enquires@bgs.ac.uk)

### **Kingsley Dunham Centre, Keyworth, Nottingham NG12 5GG**

Tel 0115 936 3241 Fax 0115 936 3488  
email [sales@bgs.ac.uk](mailto:sales@bgs.ac.uk)

### **Murchison House, West Mains Road, Edinburgh EH9 3LA**

Tel 0131 667 1000 Fax 0131 668 2683  
email [scotsales@bgs.ac.uk](mailto:scotsales@bgs.ac.uk)

### **London Information Office at the Natural History Museum (Earth Galleries), Exhibition Road, South Kensington, London SW7 2DE**

Tel 020 7589 4090 Fax 020 7584 8270  
Tel 020 7942 5344/45 email [bgs london@bgs.ac.uk](mailto:bgs london@bgs.ac.uk)

### **Columbus House, Greenmeadow Springs, Tongwynlais, Cardiff CF15 7NE**

Tel 029 2052 1962 Fax 029 2052 1963

### **Forde House, Park Five Business Centre, Harrier Way, Sowton EX2 7HU**

Tel 01392 445271 Fax 01392 445371

### **Maclean Building, Crowmarsh Gifford, Wallingford OX10 8BB**

Tel 01491 838800 Fax 01491 692345

### **Geological Survey of Northern Ireland, Colby House, Stranmillis Court, Belfast BT9 5BF**

Tel 028 9038 8462 Fax 028 9038 8461

[www.bgs.ac.uk/gsni/](http://www.bgs.ac.uk/gsni/)

### *Parent Body*

### **Natural Environment Research Council, Polaris House, North Star Avenue, Swindon SN2 1EU**

Tel 01793 411500 Fax 01793 411501  
[www.nerc.ac.uk](http://www.nerc.ac.uk)

Website [www.bgs.ac.uk](http://www.bgs.ac.uk)

Shop online at [www.geologyshop.com](http://www.geologyshop.com)

# Foreward

This report is the product of a study by the British Geological Survey (BGS) undertaken on behalf of the French radioactive waste management company Agence Nationale pour la Gestion des Déchets Radioactifs (Andra) and the European Union 7<sup>th</sup> Framework Euratom Programme under the auspices of the Fate of repository Gases (FORGE) project (Project number 230357), to examine the effect of the stress path on the hydraulic and gas transport properties of the Callovo-Oxfordian claystone.

# Acknowledgements

The study was undertaken by staff of the Minerals and Waste Programme of the BGS using the experimental facilities of the Transport Properties Research Laboratory (TPRL). Funding for the study was provided by the French radioactive waste management operator, Andra, the European Union (FORGE Project) and the British Geological Survey through its well-founded laboratory programme. The authors would like to thank the skilled staff of the Research & Development Workshops at the BGS, in particular Humphrey Wallis and Steve Upton, for their design and construction of the experimental apparatus and Neil Stacey of the BGS Core Store for his skilled preparation of the samples tested.

# Contents

<b>Foreward</b> .....	<b>2</b>
<b>Acknowledgements</b> .....	<b>2</b>
<b>Contents</b> .....	<b>2</b>
<b>Executive summary</b> .....	<b>5</b>
<b>1 Introduction</b> .....	<b>6</b>
<b>2 Experimental geometry</b> .....	<b>7</b>
2.1 Test Material .....	7
2.2 Basic physical properties .....	8
2.3 Experimental set-up .....	9
2.4 Experimental programme .....	13
<b>3 Complete test history</b> .....	<b>15</b>
<b>4 Swelling history</b> .....	<b>16</b>
<b>5 Hydraulic test</b> .....	<b>17</b>
<b>6 Gas test</b> .....	<b>18</b>
<b>7 Gas test (onset of gas flow)</b> .....	<b>19</b>
7.1 Events during constant-flow pressure ramp (Day 236 – 256) .....	19
7.2 Events during constant pressure stage (Day 256 – present) .....	22

<b>8 Interpretation and discussion.....</b>	<b>24</b>
8.1 Dilatant gas migration.....	24
8.2 Compressibility and observations of pore-pressure in CO <sub>x</sub> .....	26
<b>9 Summary .....</b>	<b>28</b>
<b>References .....</b>	<b>31</b>

## FIGURES

Figure 2-1	Sample preparation. (a) The core samples are delivered with the CO <sub>x</sub> material encased in a thin rubber material, surrounded by a cement material, and the outside of the core barrel is a plastic material. (b) The 300mm length core barrel was sub-sampled into 100mm length by dry cutting using a diamond encrusted blade. (c) Finished sample of CO <sub>x</sub> . .....	8
Figure 2-2	Schematic of the Stress Path Permeameter (SPP).....	11
Figure 2-3	Photo of the SPP apparatus. The hydraulic ram (yellow) can be seen, along with the dash-pots used to measure radial deformation of the jacketed samples. .	12
Figure 2-4	Components of the SPP. (a) The complete apparatus, showing the pressure vessel, pressure distribution board, four ISCO pumps [confining pressure, axial load, injection and back pressure], and optical encoder box. (b) Modified Hoek sleeve with brass additions that are in direct contact with the arms of the dash-pot arrangement. (c) Pressure balanced dash-pot system. The dashpot arm [4] is in direct contact with the outside of the sample jacket. The movement of this arm is recorded by a high-precision LVDT [1]. The dashpot is pressure balanced through the pressure ports marked [3]. .....	13
Figure 5	Data for complete test history. A) Pressure history, b) radial and axial displacement, c) sample strain, d) flow data and e) temperature. ....	15
Figure 6	Data for the initial swelling stage of the test history. A) radial and axial displacement, b) sample strain, and c) flow data. ....	16
Figure 7	Data for the hydraulic testing stage of the test history. A) Pressure history, b) radial and axial displacement, c) sample strain, and d) flow data. ....	17
Figure 8	Data for the gas testing stage of the test history to date. A) Pressure history, b) radial and axial displacement, c) sample strain, and d) flow data. ....	18
Figure 9	Summary of main events that occurred during the constant-pressure ramp. A & b) pressure history; c) deformation; d) axial load; e) injection pressure guard-ring; f) back-pressure flow; g) pack-pressure flow versus injection pressure. ....	20
Figure 10	Detail of the radial deformation recorded at the mid-plane of the sample at the onset of gas flow. ....	21
Figure 11	The difference between predicted gas pressure for constant flow testing and recorded pressure. Three periods within this data are seen to be affected by small temperature variations within the laboratory. However, a change in slope is seen at Day 222, which may indicate the onset of gas flow into the sample. ....	22
Figure 12	Summary of main events that occurred during the constant pressure stage. A) deformation; b) volumetric strain; c) injection and back-pressure flow; d) pressure history; e) detail of pressure at injection guard ring; e) detail of pressure at back-pressure guard ring.....	23

Figure 13 Interpretation of the onset of gas flow in CO<sub>x</sub>. A) The onset of gas flow. B) Gas reaches the injection-end guard ring and displaces water into the sample. C) A more significant feature is created causing the pressure in the guard ring to increase and the sample to start to dilate. D) Gas migration has reached the back-pressure end as seen in a rise of outflow. As more pathways are opened the sample continues to dilate. .... 25

Figure 14 Pore pressure differentials observed within the sample. A) difference between injection pressure and injection guard ring; b) difference between back-pressure and back-pressure guard ring; c) difference between injection guard ring and back pressure guard ring. .... 27

## TABLES

Table 2-1	Provisional dimensions and basic properties of the Callovo-Oxfordian claystone test material (sample SPP_CO <sub>x</sub> -2) from pre-test measurements of water content from off-cut material adjacent to the core. An assumed specific gravity for the mineral phases of 2.70 Mg.m <sup>-3</sup> (Zhang <i>et al.</i> 2007) was used in these calculations. ....	9
Table 2-2	Summary of experimental history showing stage number, description of stage, axial stress and confining stress. ....	14
Table 8-3	Summary of events that represent the migration of gas through the CO <sub>x</sub> . ....	26
Table 9-4	Summary of all events relevant to onset of gas flow through the CO <sub>x</sub> . Key: # = deflection in reading; #_ = reading has reached plateau; ↑ = sharp increase in reading; ↓ sharp decrease in reading; ↓↓ = onset of accelerated radial strain; ∧ = peak in reading; ∨ = trough in reading; Gas = evidence that gas has reached guardrings. ....	30

## Executive summary

This report describes in detail the stress-path permeameter (SPP) apparatus and the on-going second test conducted on Callovo-Oxfordian (COx) claystone from the Bure underground research laboratory (URL) in France. Funding for this study has been provided by the French radioactive waste management operator, Andra, the European Union (FORGE Project, Project number 230357) and the British Geological Survey through its well-founded laboratory programme and the Geosphere Containment project (part of the BGS core strategic programme).

The results from test SPP\_COx-2 clearly show that at the onset of gas propagation through the test sample dilatancy is observed in three radial and one axial direction. A component of this dilatancy is associated with changes in pore pressure. However, pore-pressure variation cannot account for the full amount of strain recorded and a proportion of the strain observed is the result of gas migration by dilatant pathway formation. The test is on-going and more insight will be achieved once the test is complete.



# 1 Introduction

This report introduces the data obtained from the on-going SPP\_COx-2 test. The primary purpose of this report is to introduce the evidence for dilatancy at the onset of gas flow. The report continues the experimental programme on COx as part of the European Union 7<sup>th</sup> Framework Euratom Programme Fate of repository Gases (FORGE) project (Project number 230357). Data from the first test (SPP\_COx-1) was reported in Cuss & Harrington (2010).

The objective of the experimental programme is to examine the impact of changing effective stress (e.g. caused by the construction of a disposal/storage facility) and to investigate its effects on the sealing characteristics of the Callovo-Oxfordian (COx) claystone. As such, there is a need to understand the roles of the stress tensor, the stress path and associated mechanical deformation in determining permeability changes affecting the sealing efficiency of the claystone. Under certain stress conditions, mudrock deformation will result in dilation (net volume increase) or contraction (net volume decrease). The boundary between these conditions is referred to as the dilatancy boundary and this plots as a point in the mean stress ( $p$ ) versus deviatoric stress ( $q$ ) space, or a line when specific volume ( $v$ ) is used as a third axis. Critical state mechanics shows that complex deformation can be described by a series of yield surfaces in the  $p' - q' - v$  parametric space. Calibration of this model can be undertaken by taking samples of mudrock along predefined stress paths extending to the yield surfaces while measuring the resulting changes in permeability (both aqueous and gaseous). The main output of the research will be to enhance process understanding in Engineering Disturbed Zone (EDZ) mudrock environments, through the critical examination and subsequent validity of key geomechanical relationships applied to mudrock deformation and its role in the temporal evolution of permeability during the operational and post closure repository phases.

The purpose of this experimental study is to provide quantitative data examining the mechanisms governing gas migration and the evolution of permeability during deformation. The primary objectives of this experimental study are to measure the evolution of permeability (both hydraulic and gas) of the Callovo-Oxfordian claystone subject to complex changes in stress and porewater pressure. The secondary purpose of this experimental study is to investigate the volumetric deformation that occurs during the migration of water and gas through the COx. A high precision triaxial deformation apparatus has been constructed that can reliably detect sub-micron scale deformation of the mid-plane of the test sample. This report introduces the first data achieved on this aspect of the experimental programme.

## 2 Experimental geometry

### 2.1 TEST MATERIAL

The composition of the Callovo-Oxfordian claystone (150-160 Ma) can be divided into three main constituents; clay, silt and carbonate. Wenk *et al.* (2008) reports these constituents (at the Bure site) as follows; clay 25-55 wt%, 23-44% carbonates and 20-31% silt (essentially quartz + feldspar). Clay minerals are reported to include illite and illite-smectite with subordinate kaolinite and chlorite. In the upper half of the formation the illite-smectite is disordered and contains 50-70% smectite interlayers, whilst in the lower half the illite-smectite is ordered (R=1 type) with lower contents (20-40%) of smectite interlayers (Wenk *et al.*, 2008). Beds can contain common organic matter.

Other authors report compositions similar to these. Wileveau & Bernier (2008) quote values for quartz (18%), calcite (25%), clay minerals (55%; illite-smectite ~65%, illite 30%) and kaolinite and chlorite (2%) with subordinate feldspars, pyrite and iron oxides (2%). Esteban *et al.* (2006) report 35-60% clay minerals with the remaining shared by calcite and silt. Gaucher *et al.* (2004) includes highly detailed mineralogical and chemical compositions of the sequence which are again in broad agreement with the above compositions.

The claystone was deposited under marine basin conditions during a period in which the Paris Basin was variously linked to the Atlantic and Tethyan Oceans, as well as to the London Basin and North Sea (Rousset & Clauer, 2003). Clay sedimentation is therefore considered to have two primary inputs; continental and oceanic. The claystone is over- and underlain by Oxfordian and Bathonian shelf limestones. It is primarily clayey at its base, then becomes increasingly silty and then increasingly calcareous at its top (Gaucher *et al.*, 2004). A maximum clay content zone within the clayey base has been identified; this is interpreted to mark the inflection point (and interval of maximum flooding) from a lower transgressive sequence to an upper regressive sequence (Gaucher *et al.*, 2004).

Upon receipt of the preserved T1-cell core barrels at BGS, the material was catalogued and stored under refrigerated conditions of 4°C (to minimise biological and chemical degradation) ready for future testing. The core material is delivered with a rubber material around the CoX sample, surrounded by a cement material with a plastic outer jacketing material, as seen in Figure 2-1a. Each T1-cell contains approximately 300mm of core, enough for three finished samples. The core barrel was cut into three (approximately 100mm length) using a dry-cut diamond encrusted bladed saw (see Figure 2-1b).

Following the problems reported in Cuss & Harrington (2010) in sample preparation, a modified methodology was employed. The complete core was placed in a lathe and slowly trimmed to a diameter of 56mm to get a good even surface finish and the sample ends were ground flat and parallel to minimise “end-effects” during testing. The specimen was accurately measured using a digital micrometer and weighed. Off-cuts from the coring process were weighed and oven dried to obtain an estimate of moisture content. The dimensions and provisional geotechnical properties of the specimen are given in Table 2-1.

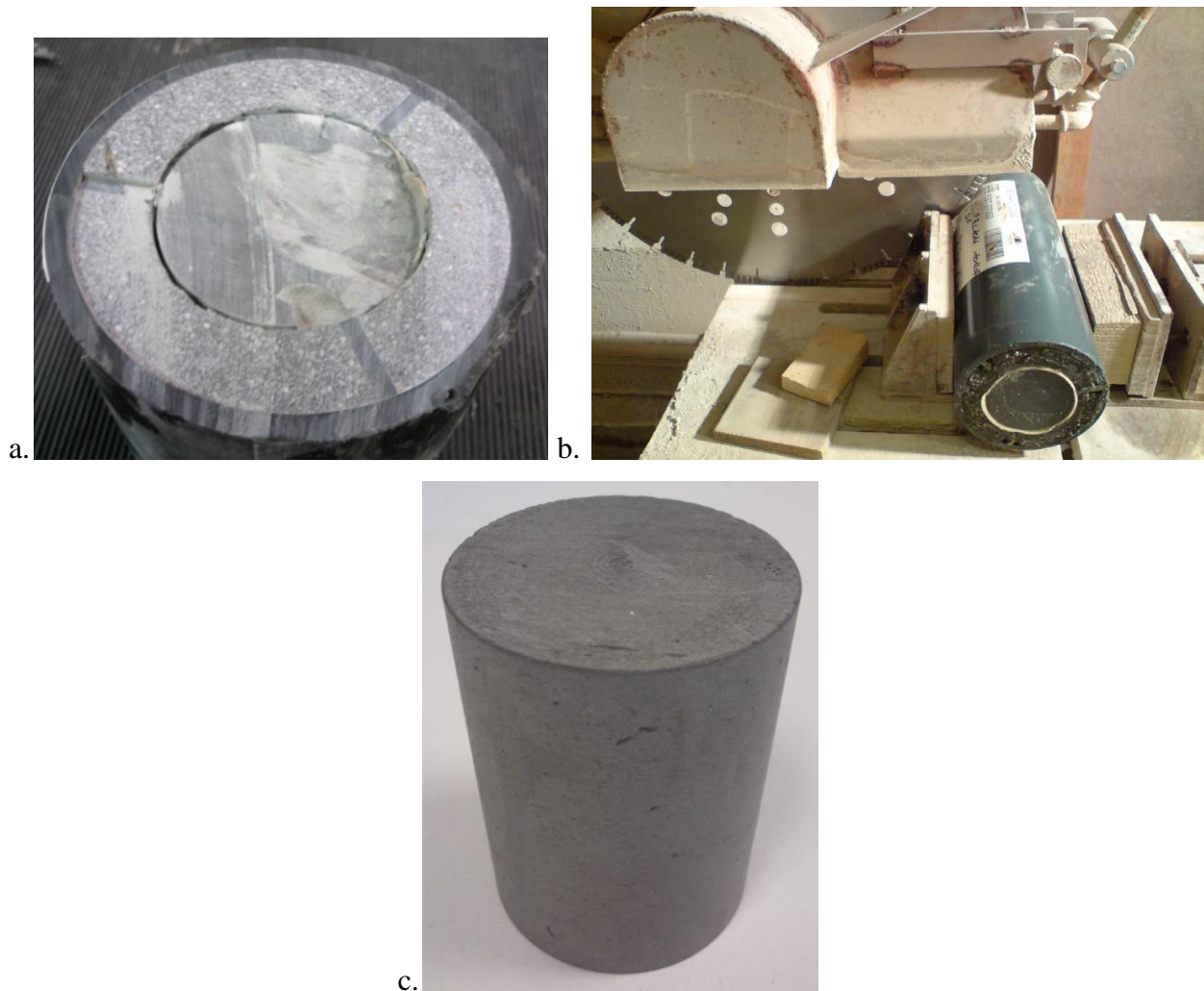


**Figure 2-1** Sample preparation. (a) The core samples are delivered with the COx material encased in a thin rubber material, surrounded by a cement material, and the outside of the core barrel is a plastic material. (b) The 300mm length core barrel was sub-sampled into 100mm length by dry cutting using a diamond encrusted blade. (c) Finished sample of COx.

The test specimen, designated SPP\_COx-2, was cut parallel to the bedding, and was taken from drilling core EST30341, dated 30/10/08 from borehole OHZ1201, T cell T1.1111, drilling interval 30.49m to 30.80m. The torque applied to the axial confining system of the T1-cell was around 18 Nm. Test sample SPP\_COx-2 is from the adjacent core barrel as test sample SPP\_COx-1.

## 2.2 BASIC PHYSICAL PROPERTIES

The starting sample was measured five times for length and nine times for diameter. The sample was weighed, which allowed bulk density to be determined. Table 2-1 shows the preliminary pre-test physical properties of the specimens based on the moisture content of the off-cuts and a grain density of  $2.70 \text{ Mg.m}^{-3}$  (Zhang *et al.*, 2007). The provisional data presented in Table 2-1 is in agreement with the generic values quoted by Zhang *et al* and for test SPP\_COx-1.

	Units	Value
<b>Sample reference</b>		SPP_COx-2
<b>Average length</b>	mm	82.45 ± 0.03
<b>Average diameter</b>	mm	55.85 ± 0.04
<b>Volume</b>	m <sup>3</sup>	2.020 × 10 <sup>-4</sup>
<b>Average weight</b>	g	495.02
<b>Density</b>	g.cc <sup>-1</sup>	2.451
<b>Grain density</b>	g.cc <sup>-1</sup>	2.7
<b>Moisture weight</b>	g	28.7
<b>Moisture content</b>	%	6.2
<b>Dry weight</b>	g	466
<b>Dry density</b>	g.cc <sup>-1</sup>	2.31
<b>Void ratio</b>		0.174
<b>Porosity</b>	%	14.8
<b>Saturation</b>	%	96

**Table 2-1** Provisional dimensions and basic properties of the Callovo-Oxfordian claystone test material (sample SPP\_COx-2) from pre-test measurements of water content from off-cut material adjacent to the core. An assumed specific gravity for the mineral phases of 2.70 Mg.m<sup>-3</sup> (Zhang *et al.* 2007) was used in these calculations.

### 2.3 EXPERIMENTAL SET-UP

The stress-path permeameter (SPP) is an evolution of the elastimeter apparatus that has been shown to perform well (Horseman *et al.*, 2005). A schematic of the SPP is shown in Figure 2-2, along with a photo in Figure 2-3. The SPP comprises 6 main components:

- 1) The specimen, surrounded by a modified flexible Hoek sleeve (Figure 2-4b) and main pressure vessel body.
- 2) Three dash pots (Figure 2-4c) that are mounted along the radial mid-plane of the sample which directly measure the radial strain of the sample. The dash pots are pressure balanced in order to reduce the force imposed upon the sample and to make sure the push-rods are not simply pushed out of the pressure vessel.
- 3) An axial load system comprising of an Enerpac single acting hydraulic ram (see Figure 2-3) pressurised by an ISCO-500 series D syringe pump. This is connected via an axial strain jig to a Global Digital Systems optical encoder for measuring linear displacement accurate to 0.003 mm. Miniture load cells are located at the piston ends to measure stress at the sample ends.
- 4) A confining pressure system using an ISCO-500 series D syringe pump allowing radial strain measurements to be calculated through volume change.
- 5) A pore pressure system comprising two ISCO-100 series D syringe pumps to create pore fluid pressure and monitor back pressure. The injection media can be either water or gas (usually Helium).
- 6) A state-of-the-art custom designed data acquisition system facilitating the remote monitoring and control of all experimental parameters.

A cylindrical rock specimen is positioned between two stainless steel platens and jacketed in a flexible Hoek sleeve to exclude the confining fluid (Figure 2-4b). The inlet and outlet zones for water flow to and from the specimen are provided by stainless-steel discs, nominally 20 mm in diameter and 3 mm depth. Guard rings of 6mm thickness and 2 mm depth are located on the outer diameter of the platens, allowing pore pressure to be measured in two locations on the faces of the sample.

The stainless steel load platens are in direct contact with the sample transmitting the axial force generated by the Enerpac ram directly to the specimen. Each platen has two ports facilitating flushing of the system and the removal of residual air prior to testing. Retaining collars and axial tie-rods lock the system components together to provide a rigid test rig, these are pre-tensioned at 300 Nm.

Axial displacement is measured using the GDS optical encoder connected to stainless steel push rods terminating a short distance behind the load-bearing face of each platen to minimise compliance effects. Data from the optical encoder is processed through a multiplexer to provide a continuous measure of axial strain. The confining system provides an indirect measurement of radial strain by monitoring changes in volume while porewater displacement is monitored via the backpressure system.

Three pressure balanced dash-pots (Figure 2-4c) are located around the radial mid-plane of the specimen. Brass push-rods are in direct contact with the outer diameter of the Hoek sleeve. Three  $10 \times 10$  mm brass plates are cemented to the outer edge of the Hoek sleeve (Figure 2-4b) in order to reduce the force the push-rods impose on the sample surface. The push rods extend to the outside of the pressure vessel, where high precision LVDTs are used to measure the displacement of the sample diameter.

Each ISCO pump controller has an RS232 serial port that allows volume and pressure data to be transmitted to an equivalent port of a 32-bit personal computer. A state-of-the-art data acquisition system was developed using National Instruments LabVIEW™ software. The system allows both remote access to test parameters and control of all ISCO pumps via a LAN based telemetry link. The software prompts the pump controller and multiplexer unit to transmit data to the computer at pre-set time intervals. Data can be downloaded at any time without physical access to the laboratory, minimising thermal variations due to personnel working in the laboratory environment.

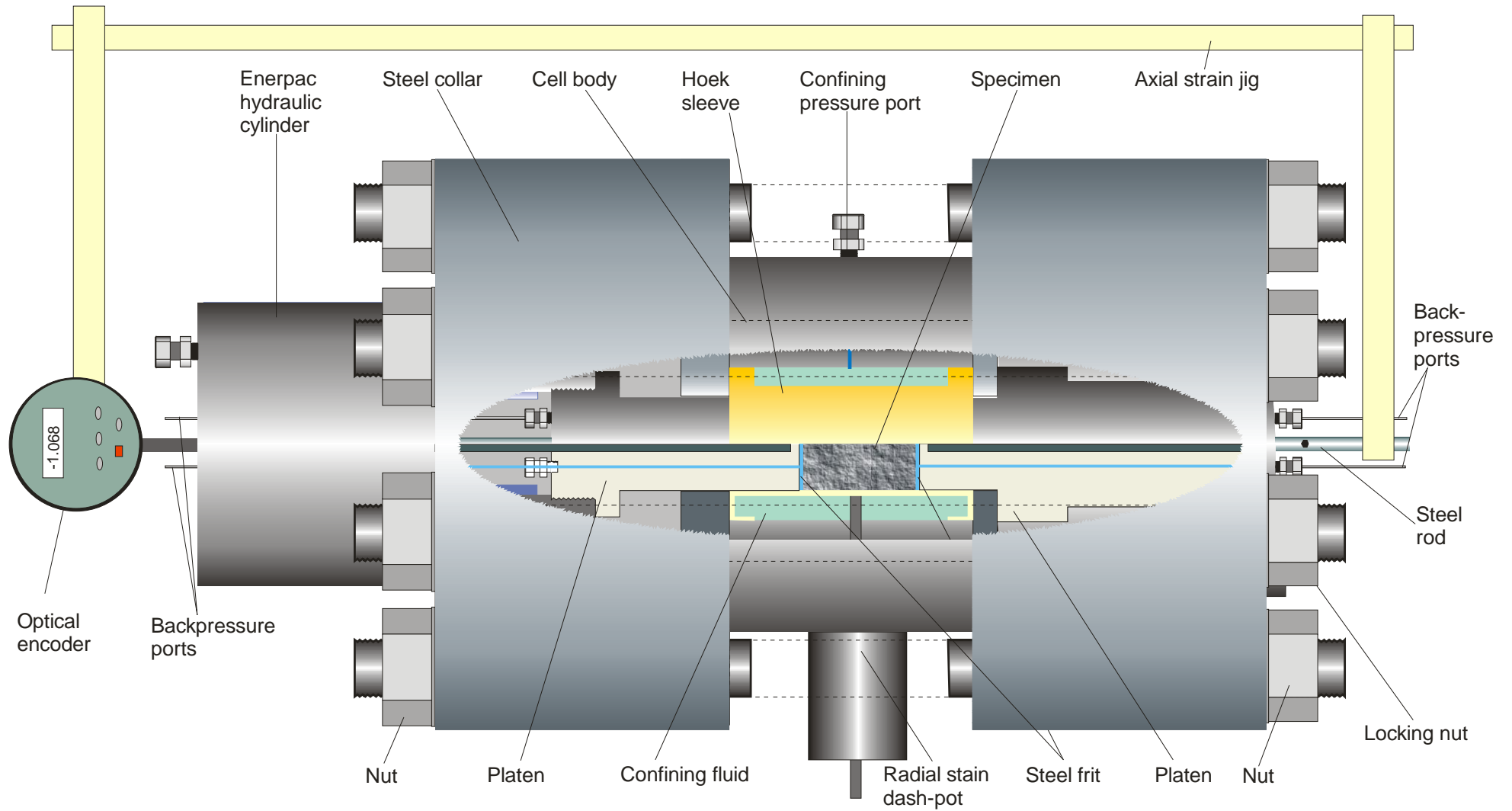


**Figure 2-2** Schematic of the Stress Path Permeameter (SPP).

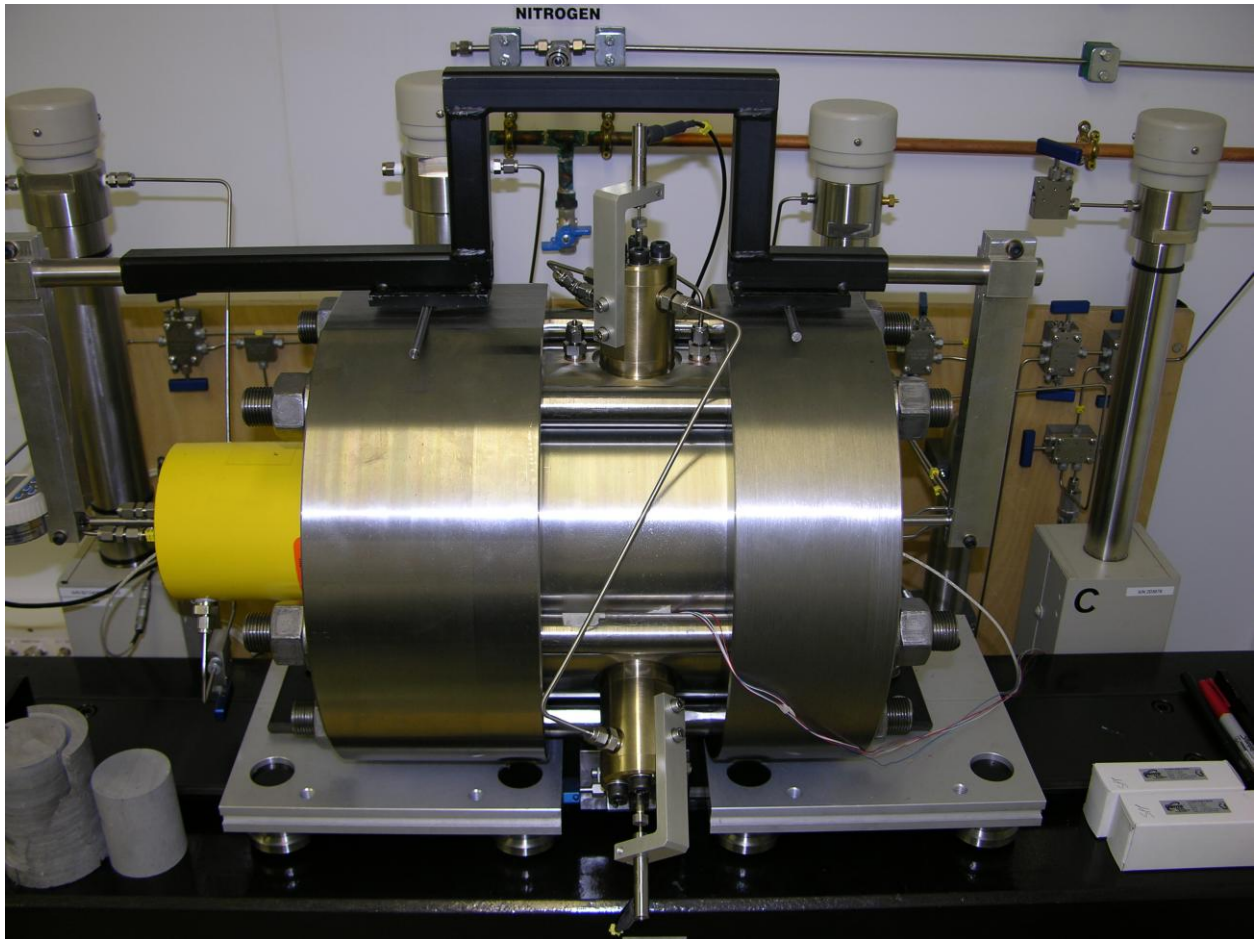


**Figure 2-3** Photo of the SPP apparatus. The hydraulic ram (yellow) can be seen, along with the dash-pots used to measure radial deformation of the jacketed samples.

### 2.3.1 Measured parameters

The SPP logging software directly records the following parameters every 2 minutes:

- SPP injection circuit pump (pressure, flow and volume)
- SPP back-pressure circuit pump (pressure, flow and volume)
- SPP axial load pump (pressure, flow and volume)
- SPP confining pressure pump (pressure, flow and volume)
- Load cell on the injection platen
- Load cell on the back-pressure platen
- Radial displacement of the sample mid-plane (Radial 1, Radial 2 & Radial 3)
- Axial displacement of the sample
- Temperature (vessel, laboratory low level and laboratory high level)

From the measured parameters, the following calculated parameters can be determined:

- Axial strain of the sample
- Radial strain of the sample
- Volumetric strain of the sample
  - From direct measurements on the sample
  - From displacement of confining fluid
- Permeability and storage capacity
- Stress state



In addition to these parameters, physical properties can be recorded prior to testing and on test completion.



**Figure 2-4** Components of the SPP. (a) The complete apparatus, showing the pressure vessel, pressure distribution board, four ISCO pumps [confining pressure, axial load, injection and back pressure], and optical encoder box. (b) Modified Hoek sleeve with brass additions that are in direct contact with the arms of the dash-pot arrangement. (c) Pressure balanced dash-pot system. The dashpot arm [4] is in direct contact with the outside of the sample jacket. The movement of this arm is recorded by a high-precision LVDT [1]. The dashpot is pressure balanced through the pressure ports marked [3].

## 2.4 EXPERIMENTAL PROGRAMME

The complete experimental programme for test SPP\_COx-2 will take the sample along the same, more detailed, stress-path as that conducted in test SPP\_COx-1 (Cuss & Harrington, 2010), but this time will include the injection of gas. Table 2-2 shows the test stages to date. Test SPP\_COx-2 is still ongoing at the time of writing this report and only preliminary results for observations of volumetric strain during the first stress-path step at the onset of gas flow are given.



Stage number	Description	Axial stress (MPa)	Confining stress (MPa)	Injection pore-pressure (MPa)	Test time at start (days)	Length of stage (days)
1	Saturation and swelling	12.5	11.5	4.5	0.1	21.7
2	Equilibration	13.0	12.5	4.5	21.8	26.1
3a	Hydraulic testing	13.0	12.5	8.5	47.9	50.1
3b	Hydraulic testing	13.0	12.5	4.5	98.0	29
4a	Gas injection ramp (constant flow)	13.0	12.5	4.5 – 9.5	127.0	35.3
4b	Gas injection at constant pressure	13.0	12.5	9.5	162.3	25.5
4c	Gas injection ramp (constant flow)	13.0	12.5	9.5 – 10	187.8	22.2
4d	Gas injection at constant pressure	13.0	12.5	10	210.0	26.1
4e	Gas injection ramp (constant flow)	13.0	12.5	10 – 10.5	236.1	18.9
4f	Gas injection at constant pressure	13.0	12.5	10.5	255.0	On-going

**Table 2-2** Summary of experimental history showing stage number, description of stage, axial stress and confining stress.

### 3 Complete test history

Figure 5 shows the test result data for the complete test history up to Day 272 on 2<sup>nd</sup> August 2011. The four stages of the test to date can be clearly seen (initial swelling stage, equilibration at *in situ* conditions, hydraulic testing and gas injection testing). Results for each section will be introduced in the following sections.

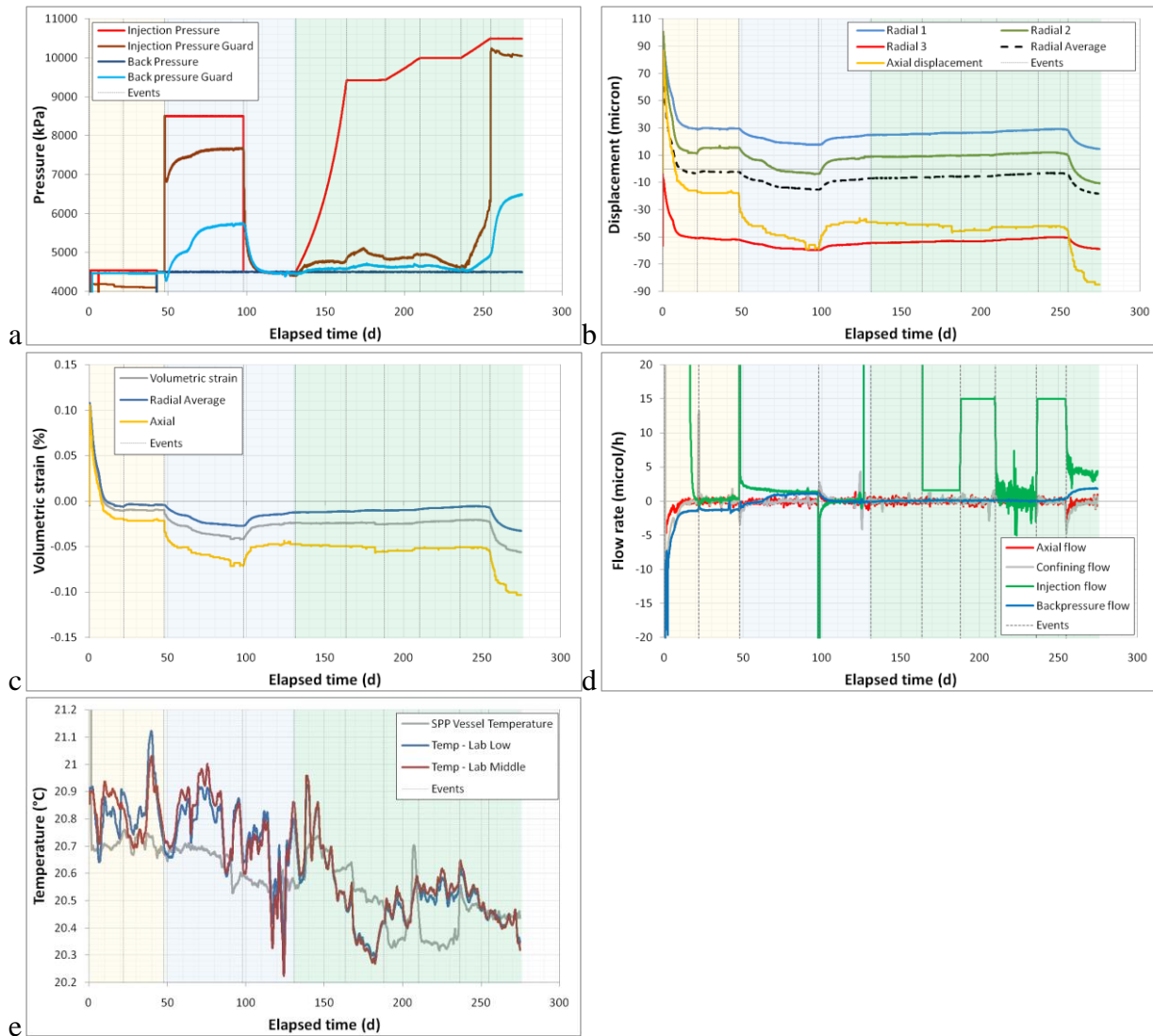


**Figure 5** Data for complete test history. A) Pressure history, b) radial and axial displacement, c) sample strain, d) flow data and e) temperature.

## 4 Swelling history

The sample was loaded axially and then confining pressure was placed on the sample. A pore pressure of 4.5 MPa was generated at both the injection and back-pressure ends of the sample and the swelling was observed for 21 days. The stress conditions were then altered to *in situ* conditions and the sample response was monitored for a further 26 days. The results are shown in Figure 6.

The initial strains are difficult to determine. The generation of confining pressure results in the closure of the Hoek sleeve around the sample onto the sample face. This appears as a large strain which may not be representative of the true deformation of the sample. Therefore the “initial” displacement recorded by the radial strain measurement devices has been removed.

Initially about 0.11 % volumetric strain is generated by the imposition of stress. The generation of pore pressure and rehydration of the sample results in approximately 0.12 % dilational volumetric strain. By Day 21 this swelling strain had equilibrated.

Injection flow in the first 15 days of testing was seen to be considerably high compared with the back pressure flow. Both pressure systems were at 4.5 MPa and so there was no reason for flow to be initiated. Several pressure couplings on the experimental apparatus were tightened and flow reduced to an almost zero flow condition; therefore this high flux can be attributed to leakages in the system. This is problematic in terms of mass balance and the exact amount of water injected into the sample is not known.

On Day 21 the stress conditions were altered to be that of the *in situ* stress state. As can be seen in Figure 6b one radial strain (Radial 2) showed contraction, whilst the other two showed no effect on changing stress state. By the end of the stage the sample had equilibrated with low flow rates being recorded and no significant time-dependent deformation.

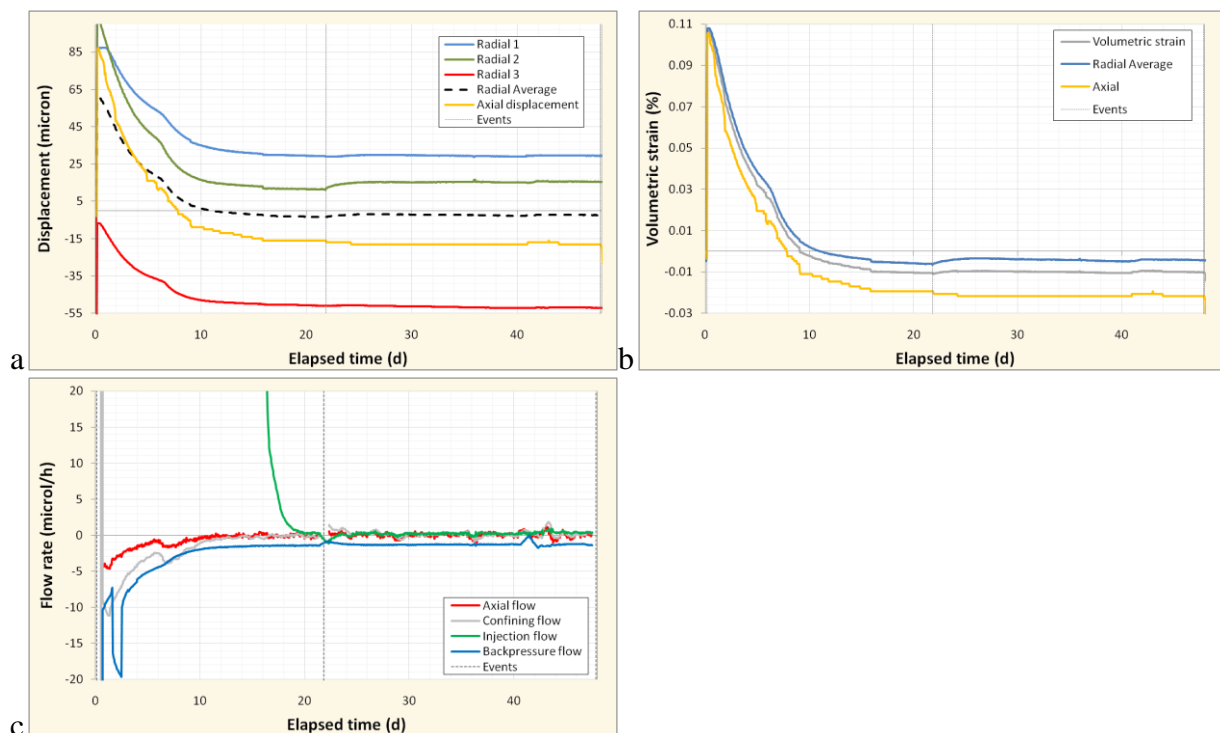


**Figure 6** Data for the initial swelling stage of the test history. A) radial and axial displacement, b) sample strain, and c) flow data.

## 5 Hydraulic test

Following the swelling stage a two-step constant head test was conducted, as shown in Figure 7. At the start of this test stage the injection pore pressure was raised to 8.5 MPa and the guard-rings were isolated. Both injection and back-pressure end guard rings showed an initial decrease in pore pressure, which within a couple of days started to recover in pressure and equilibrated. The injection end stabilised approximately 1 MPa below the injection pressure, whereas the back pressure was about 0.5 MPa above the back pressure.

The raising of injection pressure to 8.5 MPa can be seen to induce dilational strain (radially, axially and volumetrically).

Flow data (Figure 7d) shows that in the first 7 days of the hydraulic test the back-pressure flow equilibrated to a flow of approximately  $0 \mu\text{l}\cdot\text{hr}^{-1}$ . On Day 62 the backpressure flow started to increase, reaching a steady state flow of approximately  $1 \mu\text{l}\cdot\text{hr}^{-1}$  by day 87. At the onset of flow out of the sample the dilational strain of the sample started to increase (radially, axially and volumetrically). Therefore as water started to flow out of the sample the bulk sample volume increased. The onset of flow resulted in an additional 0.015 % of volumetric strain being generated (approximately  $30 \mu\text{l}$  volume). The onset of flow also resulted in the guard-ring pressured changing at both ends of the sample, with the back-pressure end having a larger increase of about 0.7 MPa. It is possible that prior to Day 62 there was a leak on the injection circuit and that this stopped. The achievement of steady state flow of  $0 \mu\text{l}\cdot\text{hr}^{-1}$  on the low pressure stage of the hydraulic test shows that no leakage was occurring later than Day 100.

Injection pore pressure was lowered to 4.5 MPa on Day 98. Over the remaining 32 days of the low pressure constant head hydraulic test stage the strain was partially recovered. This is accompanied by the slow decrease in pore pressure in the injection and back-pressure guard rings. The injection guard ring decreased much slower than the back-pressure guard ring. By the end of this test stage an additional 0.014 % of dilational strain occurred to the sample.

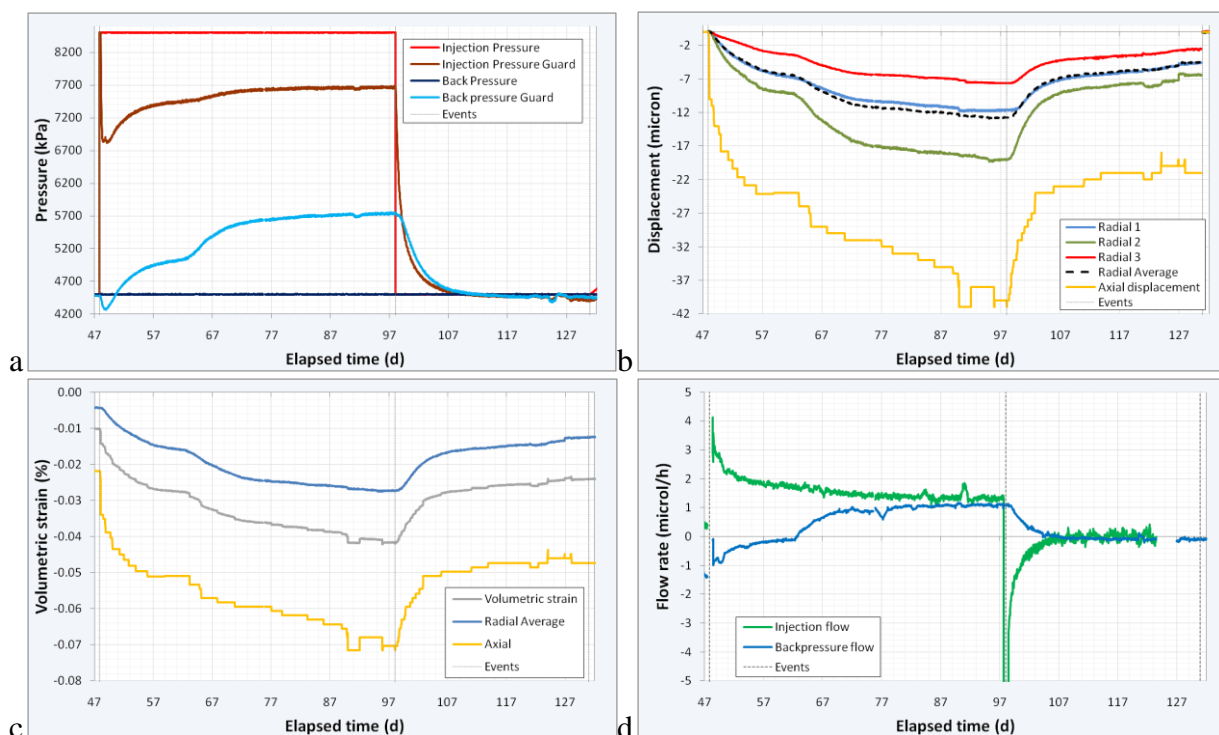


**Figure 7** Data for the hydraulic testing stage of the test history. A) Pressure history, b) radial and axial displacement, c) sample strain, and d) flow data.

## 6 Gas test

On Day 131 the gas testing phase was started, results are shown in Figure 8. The interface vessel on the injection circuit was filled with 281 ml of helium at 4.5 MPa. A constant flow pressure-ramp was initiated with a flow rate of  $190 \mu\text{l}\cdot\text{hr}^{-1}$  designed to raise pressure to 9.5 MPa in 30 days. As can be seen no flow was seen and so on Day 163 the injection pump was set to a low flow of  $1 \mu\text{l}\cdot\text{hr}^{-1}$  and held for 24 days. Prior to the switch to constant pressure the guard ring pressure data showed an increase. The injection guard ring peaked at about 5.2 MPa and slowly decayed. This corresponds with no change of inflow into, or outflow from, the sample. The kick seen in axial displacement is the result in temperature variation in the laboratory and is not a “real” sample strain.

The injection system was again changed to a constant flow pressure ramp on Day 187 to increase injection pressure by 0.5 MPa over a three week period. Again this was accompanied by subtle changes in guard-ring pore pressure, however no flow was initiated. The test was switched to constant pressure on day 210 and held for 26 days. During this period the pressure in both guard-rings decayed.

The final pressure ramp was initiated on Day 236 and similarly raised pore pressure by 0.5 MPa over a 3 week period. Almost immediately prior to reaching an injection pressure of 10.5 MPa the injection guard ring pressure greatly increased. This is introduced in more detail in the next section.

Between Day 131 and the onset of marked radial deformation (approximately Day 254) the sample showed small volumetric reduction of approximately 0.003 %.

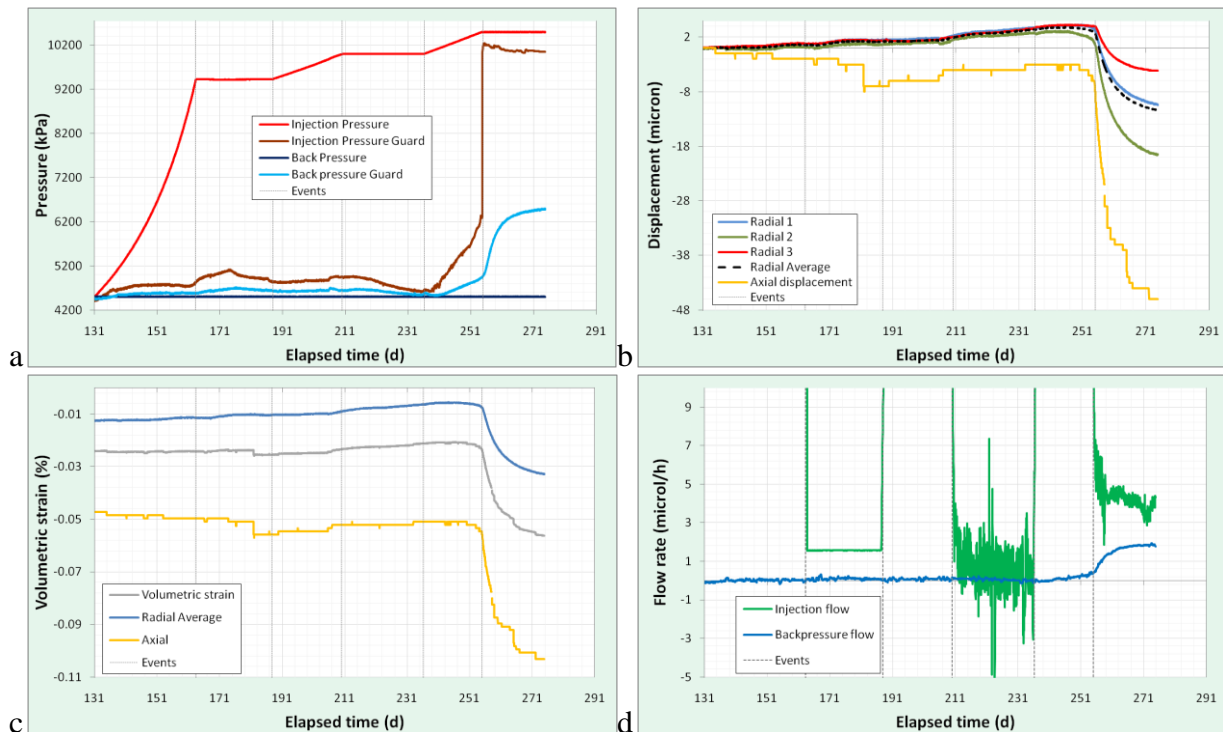


**Figure 8** Data for the gas testing stage of the test history to date. A) Pressure history, b) radial and axial displacement, c) sample strain, and d) flow data.

## 7 Gas test (onset of gas flow)

In this section we discuss the data at the time of the onset of gas flow. Figure 9 to Figure 14 shows the data in more detail between Day 230 and Day 280. In order to distinguish the subtle responses related to the onset of gas flow all data were closely examined and “events” were recorded, these are summarised in Table 9-4. These observations allow decoupling of the influence of temperature variation on any recorded results and allow the coupling between parameters to be determined. The “exact” timing of the events may include a certain degree of subjectivity. However, we have attempted to be consistent in the way events have been determined. All events are displayed on Figure 9 to Figure 14.

### 7.1 EVENTS DURING CONSTANT-FLOW PRESSURE RAMP (DAY 236 – 256)

The test was switched to constant flow in order to increase the gas injection pore pressure from 10 MPa to 10.5 MPa. All data suggested that flow had not initiated at 10 MPa. Figure 9 summarises the main events that occurred during constant-flow pressure ramp.

During the constant pressure ramp it can be seen that pressure in the injection guard ring started to increase from about Day 235.9 onwards (Figure 9a). This appears to correspond with unexplained behaviour in the load cells (Figure 9d). In the injection end this device, which in Cuss & Harrington (2010) was believed to be faulty, showed a slow decline in reading and at the point where the injection guard ring started to increase a marked jump in (uncalibrated) load cell reading is observed. The exact timing of this event was Day 237.32.

It is difficult to determine precisely when pore pressure in the back-pressure guard ring starts to increase (Figure 9b), but there was at least a one day lag compared with the injection guard ring pressure event and occurred at about Day 240.5. What is clear is that the rate of increase in pressure at the back-pressure end of the sample is much less than that at the injection end. It can also be seen that the pressure increase at the injection end shows considerable instability, whereas at the back pressure end the increase is much more smooth. This suggests that the increase at the injection end is as a result of gas migration to the guard rings, whereas the change at the back-pressure end is a hydromechanical response to effective stress changes.

Between Day 237 and Day 254.7 the pressure in the injection guard ring increased from approximately 4.6 MPa to 6.3 MPa, whilst in the back pressure guard ring the pressure increased from 4.5 MPa to 4.9 MPa. At Day 254.7 pressure in the injection guard ring increased significantly from 6.3 MPa to a peak of 10.5 MPa (Figure 9a and Figure 9e). As can be seen in Figure 9e the pressure increase was rapid (2 minute interval between data points) with pressure increasing greater than 3.5 MPa within a period of 1 hour.

Figure 9c shows the deformation data during the pressure ramp stage. As can be seen, from day 230 to 245 the radial deformation showed that the sample was slowly compacting. It should be noted that during this 15 day period the average radial deformation was approximately 1 micron. However, careful examination of this data shows several changes of slope in all three radial measurements. At Day 239.8 all three radial measurements show a deflection in their rate of change (see Figure 10). This is most pronounced in Radial 2 which reaches a plateau at this time. Radial 3 reaches plateau at Day 243.5, a time which corresponds with the start of negative (dilatant) strain being shown by Radial 2. Radial 1 does not plateau in the same manner as Radial 2 and 3, although it does peak at Day 250. Therefore the first indication of dilatancy was observed at Day 239.8 for Radial 2, Day 243.5 for Radial 3, and Day 250.21 for Radial 1.

It can be seen in Figure 9c and Figure 10 that the onset of accelerated dilatant deformation occurs at Day 254 for Radial 2, Day 254.7 for Radial 1, Day 255.1 for Radial 3 and 265.03 for Axial strain. What can also be seen is that by Day 256 the rate of change of all three radial strain sensors is similar. This suggests that initial flow through the sample was probably localised

through the centre of the sample, but with time the flow homogenised and strain evenly distributed through the radial mid-plane.

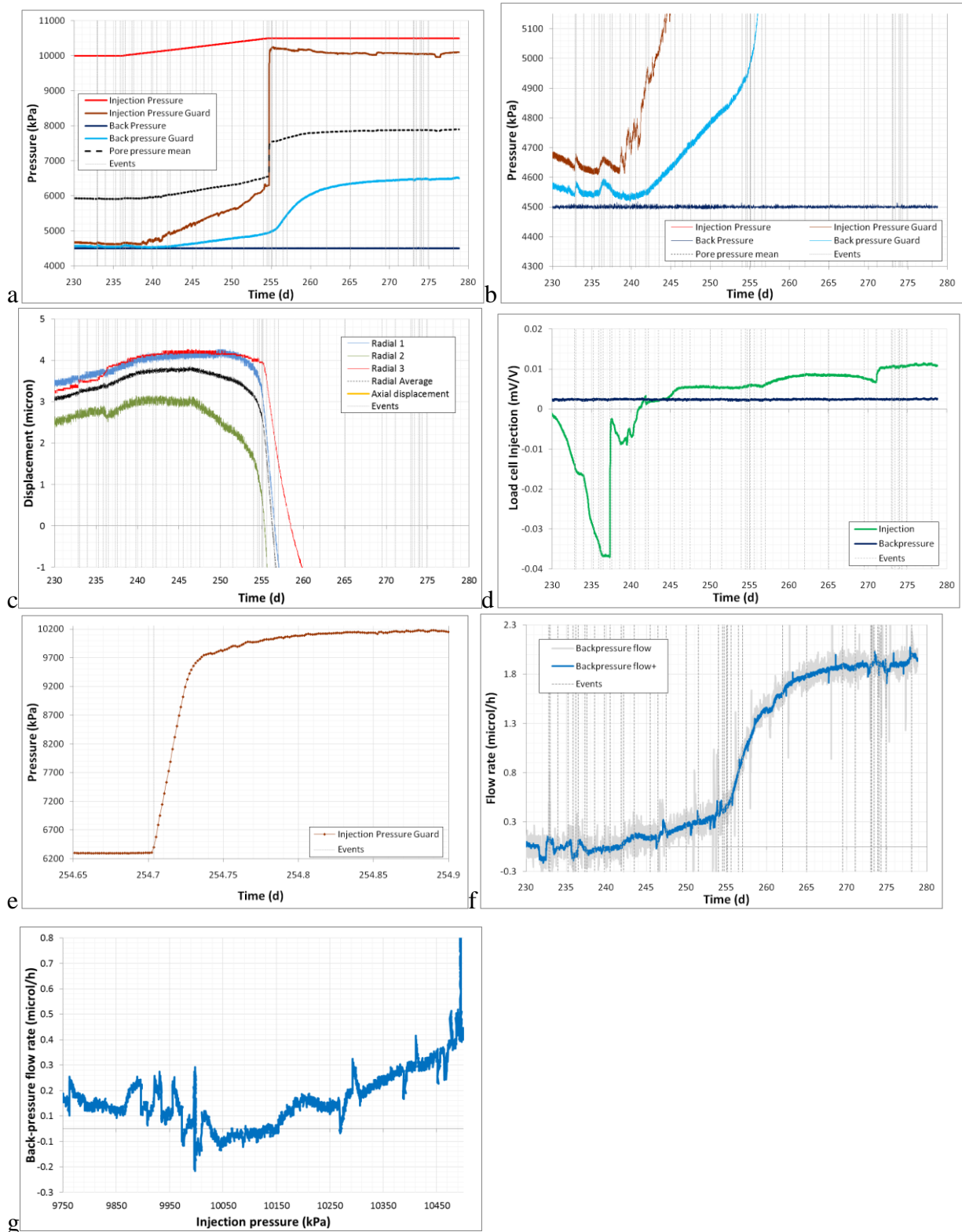


**Figure 9** Summary of main events that occurred during the constant-pressure ramp. A & b) pressure history; c) deformation; d) axial load; e) injection pressure guard-ring; f) back-pressure flow; g) pack-pressure flow versus injection pressure.



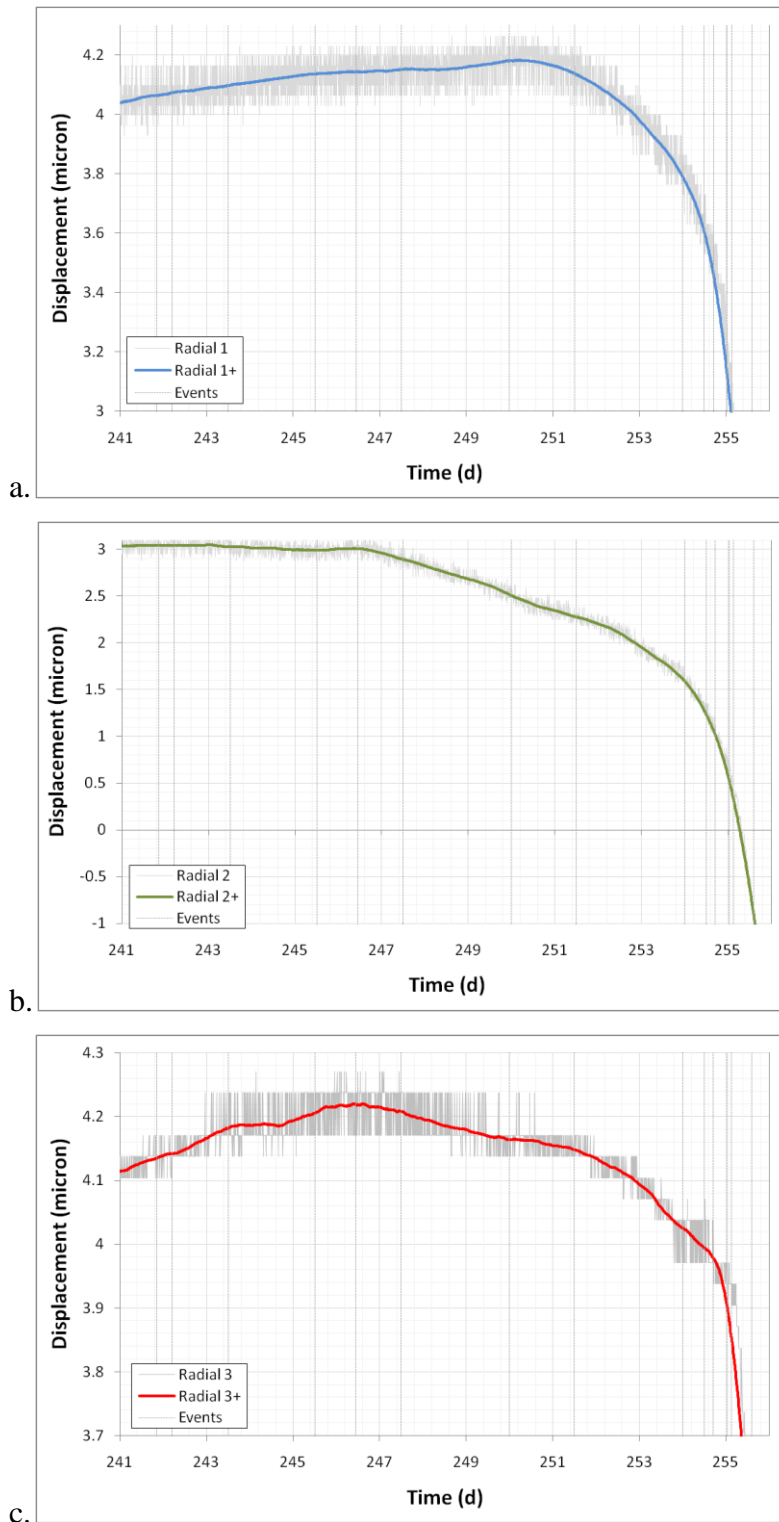


**Figure 10** Detail of the radial deformation recorded at the mid-plane of the sample at the onset of gas flow.

Taking all observations into account it can be suggested that gas started to flow into the COx on Day 237.32 with gas moving to the location of the load cell. This occurred at an injection pressure of 10.04 MPa. This observation fits with the timing of pressure changing in the injection guard ring (Day 238.55). However, as both the injection-end loadcell and guard rings are a distance from the injection point, it is suggested that gas entry occurred prior to Day 237.32. Figure 9g shows the relationship between injection pressure and back-pressure flow. This shows



that flow started to increase at an injection pressure of 10.15 MPa. Therefore all observations suggest that the gas entry pressure was approximately 10.1 MPa.

All data were carefully examined between Day 200 and Day 237.32 for any evidence of gas entry. It should be clearly noted that the laboratory experienced several small ( $\sim 0.1$  °C) temperature variations during this period. Small variations in laboratory temperature are seen to influence the response of several sensors in such a way that the effect cannot be removed by careful calibration. Therefore it is difficult to determine the onset of gas flow with a high degree of confidence. During constant flow experimentation the onset of flow can be suggested by comparing the difference between predicted gas pressure from the ideal gas law and observed gas pressure; this data is shown in Figure 11. It can be seen that between Day 202 and Day 211.5 is affected by a  $0.25$  °C temperature variation in the laboratory. At the injection pressure the variation recorded is approximately equal to that predicted by the ideal gas law. However, Figure 11 shows a change in slope at Day 220, which corresponds with a significant deflection of the injection-end load cell at Day 221.875. Therefore, we suggest that Day 221.875 represents an early gas entry event.

It is suggested that gas propagated along the end of the sample, with the behaviour of pressure response at the guard ring suggestive of the presence of gas. The pressure response at the back-pressure end of the sample also suggests that gas reached both the filter and guard-rings. The symmetry of the radial deformation suggests that gas propagated through the centre of the sample, as does the timing of pressure changes in the filter and BGR. Therefore, sidewall flow can be discounted and the observed gas propagation was through the body of the sample and the radial flow observed was as a result of bulk sample dilation and not inflation of the Hoek sleeve.

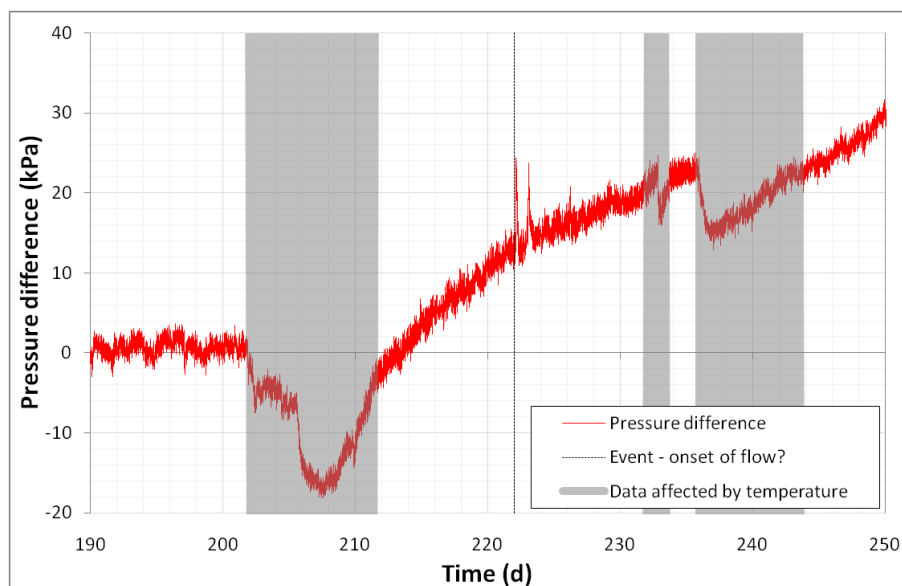


**Figure 11** The difference between predicted gas pressure for constant flow testing and recorded pressure. Three periods within this data are seen to be affected by small temperature variations within the laboratory. However, a change in slope is seen at Day 222, which may indicate the onset of gas flow into the sample.

## 7.2 EVENTS DURING CONSTANT PRESSURE STAGE (DAY 256 – PRESENT)

The injection pressure was changed from constant flow to constant pressure once dilatant deformation had been identified. This change occurred at Day 255.06 soon after the significant pressure increase in the injection pressure guard ring had occurred. Figure 12 summarises the main events that occurred during the constant pressure stage.

As seen in Figure 12a and Figure 12b marked deformation occurred following the onset of gas flow. Figure 12a shows that a total of 42 microns of length dilation occurred. The average radial dilation was approximately 15 microns. This represents a total volumetric strain of 0.035 % or 71  $\mu\text{l}$  change in sample volume.

Figure 12c shows the flow data for the injection and back-pressure ends of the sample. Following the switch from constant flow to constant pressure the injection end flow decayed initially to a flow rate of 4.7  $\mu\text{l}\cdot\text{hr}^{-1}$  at Day 261. However, flow slowly decreased so that by Day 278 flow had decreased to approximately 3.2  $\mu\text{l}\cdot\text{hr}^{-1}$ . During the same period the back pressure flow increased to a steady 2  $\mu\text{l}\cdot\text{hr}^{-1}$ .

Figure 12d to Figure 12f show the pressure response of the sample. As can be seen, the injection guard-ring peaked at a pressure of 10.23 MPa and slowly decayed. The nature of this decay is chaotic and indicative of unstable gas pathways. By Day 278 the pressure was 10.1 MPa. The pressure in the back-pressure guard ring (Figure 12f) showed an even increase in pressure. It can be seen that the increase in pressure started to become unstable from Day 273 onwards. This may indicate that gas had migrated as far as the back pressure guard ring. However, we cannot determine whether pressure changes are as a result of the presence of water or gas.

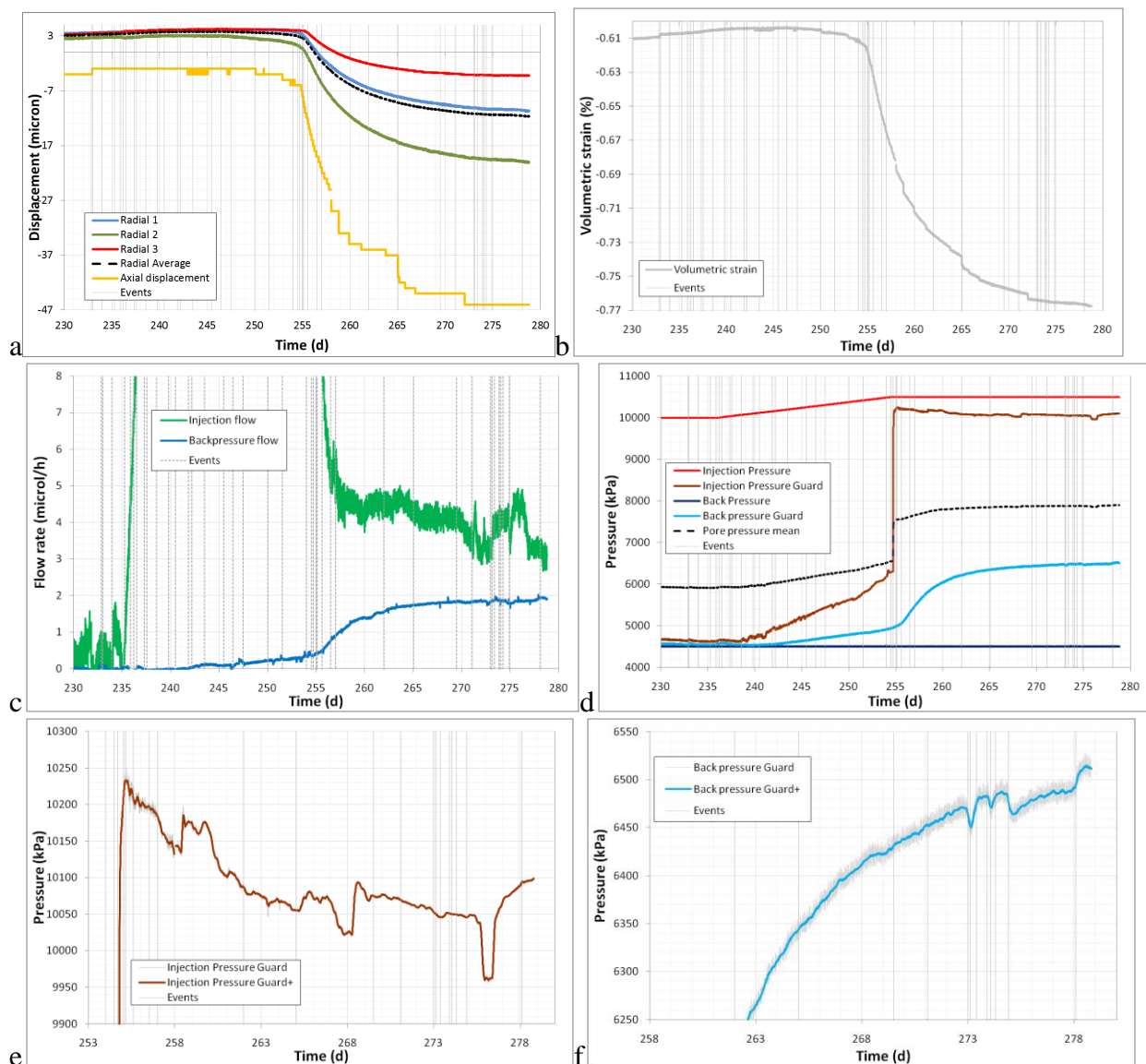


**Figure 12** Summary of main events that occurred during the constant pressure stage. A) deformation; b) volumetric strain; c) injection and back-pressure flow; d) pressure history; e) detail of pressure at injection guard ring; e) detail of pressure at back-pressure guard ring.

## 8 Interpretation and discussion

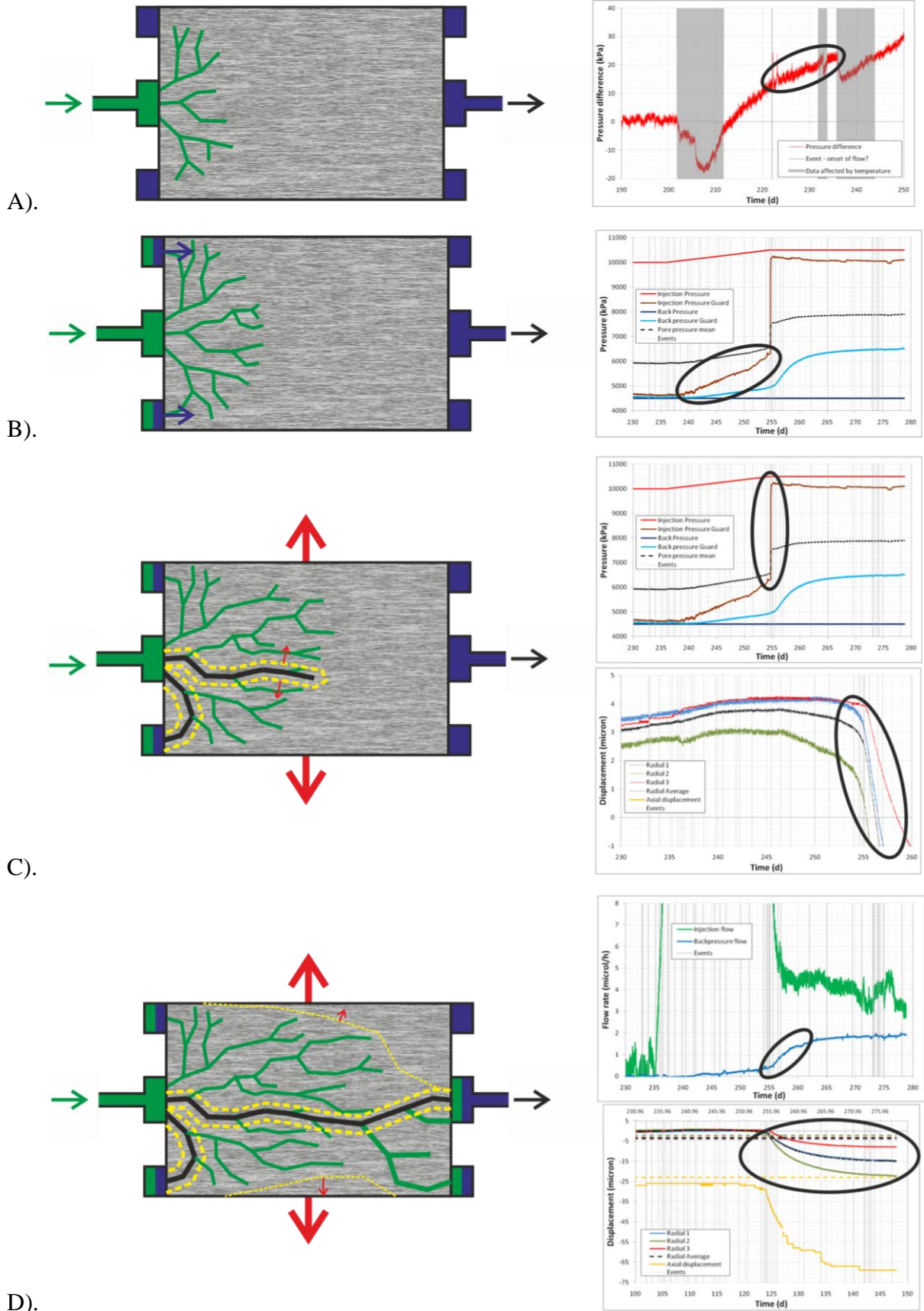
### 8.1 DILATANT GAS MIGRATION

Figure 13 shows the interpretation of the onset of gas migration in COx. The data suggest that the first gas entry into the sample occurred at Day 220 when the gas injection pressure was 10 MPa, this was seen as gas reaching the injection-end load cell. At this time the experiment was operated as constant pressure and evidence suggests that gas reached the load-cell, but did not propagate significantly further. A second event was recorded by the load cell at Day 237.32, with pressure increasing in the injection guard ring at Day 238.55. A day later at Day 239.8 the first indication of deformation was recorded at the mid-plane array of radial strain measurement devices. Deformation continued and accelerates approximately 15 days later.

**Stage 1 of gas migration:** Figure 13a shows the first stage of gas migration. At about Day 220 gas started to enter the sample when the gas injection pressure was 10 MPa. Gas migrated as far as the load-cell, where it was identified as an anomalous reading. The onset of gas migration may be indicated by a change in slope of the comparison of predicted gas pressure versus observed pressure. It is probable that gas has migrated along a single bedding layer of the COx as the current test sample is oriented parallel to bedding. Gas propagation is along dilatant pathways that exploit the pore network of the material. The pathways can be visualised as “ruptures” in the pore network. Around each pathway the fabric will compress, which may lead to localised movement of water away from the pathways.

**Stage 2 of gas migration:** Figure 13b shows the second stage of gas migration. Gas propagation throughout the sample is migrating further and has reached the corner of the sample, as seen by the onset of pressure rise at the guard ring. The geometry of the SPP apparatus means that gas is injected horizontally at one end of the sample, whereas in other apparatus gas is injected at the bottom of the sample. As a result when gas reaches the injection guard-ring it will displace water from the guard-ring into the sample until the guardring is saturated with gas. This means that early in the gas migration water is being displaced into the sample, which will result in swelling if the sample is not fully saturated. This stage is identified by a slow increase in injection guard ring pressure. The start of the stage occurred at Day 237.32 with a second anomalous reading in the injection-end load cell signifying the movement of gas. Pressure in the guard-ring started to increase at Day 238.55. A day later at Day 239.8 the first indication of deformation was recorded at the mid-plane array of radial strain measurement devices. This initial strain may have been as a consequence of water expulsion from the guard ring and small amounts of sample swelling.

**Stage 3 of gas migration:** Figure 13c shows the third stage of gas migration. A large increase in pore pressure at the injection guard ring occurred at Day 238.55 and is likely to be the result of a major conductive feature being formed in the sample. As this propagated through the sample it resulted in an acceleration of dilatant deformation. It can be seen that the acceleration of deformation at the midplane first occurs 32 days after the first sign of gas migration at Radial 2. Dilatant deformation increase occurs 0.7 days later in Radial 1 and a further 0.4 days later in Radial 3. However, axial deformation does not start to accelerate until 11 days after Radial 2. If all of the observed radial deformation was as a result of water being displaced from the guard-ring into the sample it would be expected that axial deformation would have reacted first. Therefore the observed dilatancy can not be described completely as caused by swelling. Stage 3 also shows the onset of out-flow of fluid from the sample and therefore must signify the gas movement. If all deformation was explained as derived from swelling this would not result in outflow from the sample. Therefore, even though the experimental geometry is likely to result in swelling the majority of observed deformation is caused by the dilatant propagation of gas along pathways.



**Figure 13** Interpretation of the onset of gas flow in COx. A) The onset of gas flow. B) Gas reaches the injection-end guard ring and displaces water into the sample. C) A more significant feature is created causing the pressure in the guard ring to increase and the sample to start to dilate. D) Gas migration has reached the back-pressure end as seen in a rise of outflow. As more pathways are opened the sample continues to dilate.

**Stage 4 of gas migration:** Figure 13d shows the fourth stage of gas migration. Gas has propagated through the sample as far as the back-pressure end. The onset of gas reaching the back-pressure guard ring at Day 273 indicates that gas is now moving throughout the entire length of the sample. During this stage the sample continues to dilate, which may indicate that the number of gas pathways is increasing.

Observed events (see Table 8-3) show that gas reached the injection guard-ring at Day 238.55, dilatancy was first seen at the mid-plane at Day 239.8 and the back-pressure guard ring started to increase at Day 240.5. This means that the pressure pulse propagates at a rate of approximately 37.6 mm/day or 1.6 mm/hr. This is interpreted as being a hydro-mechanical response and is created by a change in effective stress as gas starts to propagate into the sample.

	Event	Time (Days)	Distance from injection (mm)	Flow ( $\mu\text{m}\cdot\text{hr}^{-1}$ )
Hydro-mech	Gas inferred at load cell location	237.07	2	/
	Pressure rise in injection guard-ring	238.55	12	(675)
	First evidence of dilatation at mid-plane	239.8	41.25	(1250)
	Pressure rise in back-pressure guard-ring	240.5	82.5	(2000)
Gas migration	Gas inferred at load cell location	237.07	2	/
	Significant jump in pressure at guard ring	254.7	12	28.3
	Onset of accelerated mid-plane dilation	255	41.25	95.9
	Onset of gas at back-pressure guard ring	273	82.5	98.4

**Table 8-3** Summary of events that represent the migration of gas through the COx.

The acceleration of strain at the mid-plane occurred at approximately Day 255, whereas pressure at the back-pressure guard ring initiated at day 240.5 (nearly 15 days previous). This suggests that the back-pressure response is a hydromechanical response, whereas the accelerated dilatation is one of gas movement. The pressure increase in the injection pressure guard-ring is unstable and this is indicative of gas propagation, whereas the pressure increase at the back-pressure guard ring is gradual and suggests that this response is not indicative of gas reaching the back-pressure end of the sample and is the result of the hydromechanical coupling of the sample. Gas is inferred as reaching the back-pressure end at Day 273. As shown in Table 8-3, the acceleration of dilation caused by the propagation of dilatant gas pathways at the midplane and onset of gas reaching the back-pressure end give a gas propagation rate of approximately 100 microns/hour. This means that per annum gas will have moved 0.85 m.

Our interpretation has three components; 1) a response caused by the expulsion of water from the injection guard ring due to the geometry of the test set-up and the resultant swelling of COx; 2) a hydro-mechanical response of the COx as a result of the change of pore pressure from ambient (4.5 MPa) to the injection gas pressure (10 MPa); 3) a dilatant response as gas propagates through the sample. It is difficult to decouple all three components, but it is difficult to interpret the data in terms of just two-phase flow concepts.

## 8.2 COMPRESSIBILITY AND OBSERVATIONS OF PORE-PRESSURE IN COX

The injection of gas into the COx will increase the pore pressure within the sample from 4.5 MPa to the gas injection pressure (approximately 10.5 MPa). This increase of pore pressure



in 6 MPa can be viewed as being a change in effective stress on the overall sample of the same amount.

Water is a compressible medium with a bulk modulus of 2.2 GPa. The starting moisture content of the sample was calculated to be 28.7 g (i.e. 28.7 ml). The expected change in volume of water for this pressure change can be calculated from:

$$K = -V \frac{dP}{dV}$$

where K is the bulk modulus (2.2 GPa), V = volume of water (28.7 ml), dP is the change in pressure (6 MPa) and dV is the resultant volume change. Therefore:

$$dV = -V \cdot \frac{dP}{K}$$

This gives a change in volume as a result of pressure change of 78  $\mu\text{l}$ . This is very similar to the total sample deformation recorded of 71  $\mu\text{l}$ .

Figure 14 shows interesting data about the large pressure differentials observed within the COx. Figure 14a shows the difference between the injection pressure port and the injection-end guard-ring. It should be noted that the distance between these is merely 12 mm between the 20 mm diameter injection frit and 6 mm-wide guard ring. As seen the pressure difference was in excess of 5.3 MPa, which represents a pressure gradient in excess of 400  $\text{MPa}\cdot\text{m}^{-1}$ , or 40 km of head. It can be seen that even after the pressure increased in the guard-ring there is still a pressure differential of a few hundred kilopascals.

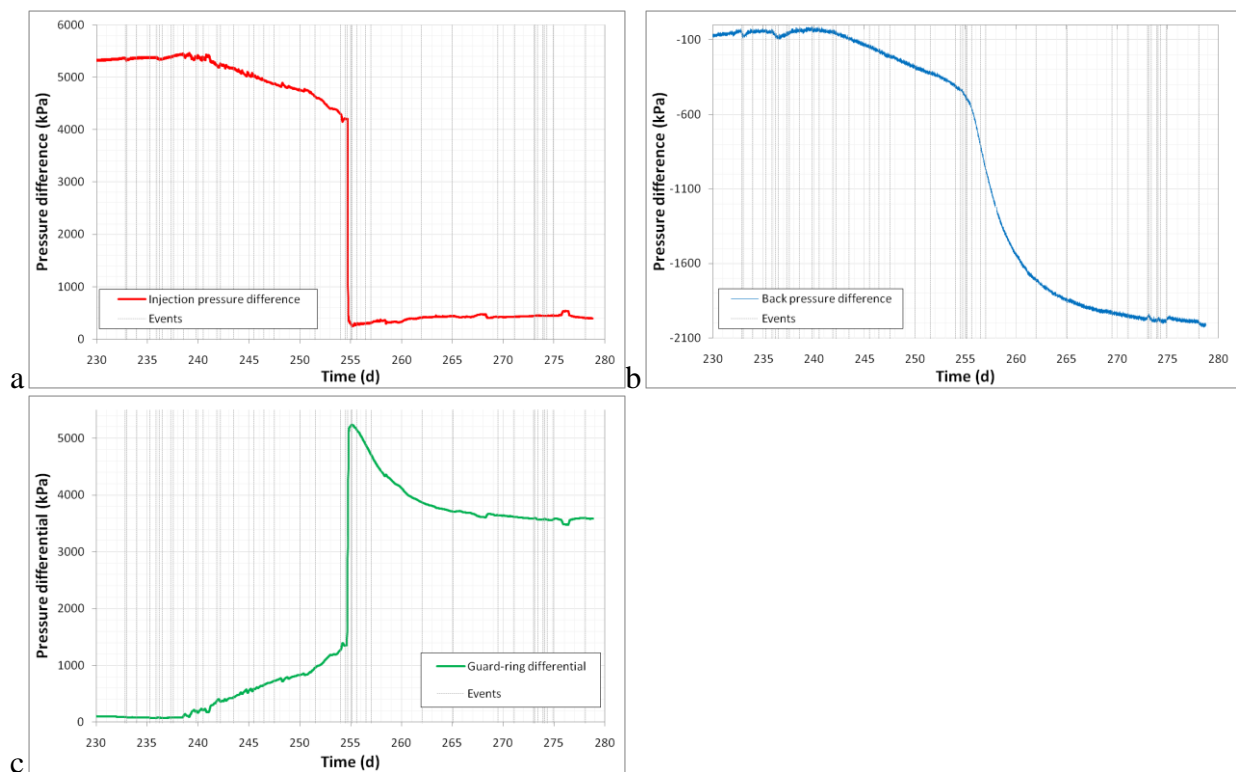


**Figure 14** Pore pressure differentials observed within the sample. A) difference between injection pressure and injection guard ring; b) difference between back-pressure and back-pressure guard ring; c) difference between injection guard ring and back pressure guard ring.

The pressure differential is not as pronounced at the back-pressure end of the sample (Figure 14b), where initially a very small differential is observed, which results in a difference of

approximately 2 MPa, which represents a pressure gradient in excess of  $160 \text{ MPa.m}^{-1}$ , or 16 km of head.

Marked pressure differential is observed between the injection and back-pressure ends of the sample at the guard rings (Figure 14c). This differential peaks at a value greater than 5 MPa, representing a pressure gradient of  $65 \text{ MPa.m}^{-1}$ , or 6.5 km of head. This differential pressure decays to a steady 3.5 MPa.

The pressure differential observed within COx during testing (as seen in hydraulic and gas testing) leads to very high pressure differentials that appear to be very stable. One of the main tenets of rock deformation is that of the law of effective stress, where the stress acting on a sample can be viewed as the total stress minus the pore pressure (Terzaghi's law of effective stress). It has been well documented that soil-like materials do not perfectly follow Terzaghi's Law, but this can be modified by a constant. The observed pore pressure within the current test leads to the question what is the effective stress acting on the sample? We have four different measures of pore pressure (injection, back-pressure, injection guard-ring, back-pressure guard-ring) and at all times of the experiment these are showing different readings, partly as a result of the boundary conditions imposed on the sample. However, it is clear that COx can accommodate very high stable pressure gradients over very small distances and this is problematic in trying to describe deformation in terms of effective stress.

The observed differences in pore pressure show that the entire water content of the sample has not undergone a 6 MPa reduction in pressure. A mean pore pressure of 7.9 MPa is observed at the end of the report period, which gives a change in average pore pressure of 3.4 MPa. This would give an elastic deformation of  $40 \mu\text{l}$ . Therefore the full deformation seen by the sample cannot be explained by elastic deformation of the sample water alone.

## 9 Summary

In this update report we have introduced data from the on-going test SPP\_COx-2.

During the initial pressurization of the sample about 0.11 % volumetric strain was observed. The generation of pore pressure and rehydration of the sample results in approximately 0.12 % dilational volumetric strain. By Day 21 this swelling strain had equilibrated.

A two-stage constant head test was conducted; pore pressure was raised to 8.5 MPa and the guard-rings were isolated. Both injection and back-pressure end guard rings showed an initial decrease in pore pressure, which within a couple of days started to recover in pressure and equilibrated. The injection end stabilised approximately 1 MPa below the injection pressure, whereas the back pressure was about 0.5 MPa above the back pressure. Flow data shows that in the first 7 days of the hydraulic test there was no flow at the back-pressure end of the sample. On Day 62 the backpressure flow started to increase, reaching a steady state flow of approximately  $1 \mu\text{l.hr}^{-1}$  by Day 87. At the onset of flow out of the sample the bulk sample volume increased, resulting in an additional 0.015 % of volumetric strain being generated (approximately  $30 \mu\text{l}$  volume). The onset of flow also resulted in the guard-ring pressure changing at both ends of the sample, with the back-pressure end having a larger increase of about 0.7 MPa. Injection pore pressure was lowered to 4.5 MPa on Day 98. Over the remaining 32 days of the low pressure constant head hydraulic test stage the strain was only partially recovered. This was accompanied by the slow decrease in pore pressure in the injection and back-pressure guard rings. The injection guard ring decreased much slower than the back-pressure guard ring. By the end of this test stage an additional 0.014 % of dilational strain occurred. This data has not yet been modelled in order to establish the hydraulic conductivity and storage of the starting material.

Gas testing was initiated on Day 131, with gas entry achieved after three constant-flow ramp stages. Gas entry first occurred on Day 220 with an anomalous reading in the load cell at Day

221.875 signifying that gas had propagated to this sink. No further gas propagation seems to have occurred during this constant pressure stage. The test was changed to constant flow in order to increase gas injection pressure from 10 MPa to 10.5 MPa pressure. A second response was seen in load cell reading at Day 237.32. This suggests that the first gas propagation event pathways closed. A day after the load cell reading response the pressure in the guard ring started to increase, a day after this the first indication of deformation at the mid-plane was seen. The following day the pressure in the back-pressure guard ring increased. These changes are interpreted as being a hydro-mechanical response to the onset of gas migration and the displacement of water from the injection guard ring due to the geometry of the test apparatus.

Gas migration was seen to result in an accelerated dilation at the mid-plane that cannot be described by the mechanical response of a change in effective stress. This suggests that gas migrated at a rate of approximately 100 microns/hour through the sample and reached the back-pressure guard ring after 18 days. The response of the sample suggests that gas has migrated along dilational pathways. Marked deformation occurred following the onset of gas flow with a total of 42 microns of length dilation occurring and an average radial dilation of approximately 15 microns. This represents a total volumetric strain of 0.035 % or 71  $\mu\text{l}$  change in sample volume.

Following the switch from constant flow to constant pressure the injection end flow decayed initially to a flow rate of 4.7  $\mu\text{l}\cdot\text{hr}^{-1}$  at Day 261. However, flow slowly decreased so that by Day 278 flow had decreased to approximately 3.2  $\mu\text{l}\cdot\text{hr}^{-1}$ . During the same period the back pressure flow increased to a steady 2  $\mu\text{l}\cdot\text{hr}^{-1}$ . The injection guard-ring peaked at a pressure of 10.23 MPa and slowly decayed. The nature of this decay is chaotic and indicative of unstable gas pathways. By the Day 278 the pressure was 10.1 MPa. The pressure in the back-pressure guard ring showed an even increase in pressure. It can be seen that the increase in pressure started to become unstable from Day 272 onwards. This may indicate that gas had migrated as far as the back pressure guard ring.

The pressure differential observed within COx during testing (as seen in hydraulic and gas testing) leads to very high pressure differentials that appear to be very stable. This is problematic in trying to describe deformation in terms of effective stress. The response of the COx suggests that mechanical responses to stress changes are very localised and that gas pathways are not distributed throughout the complete pore network, i.e. gas is propagating along localised dilatant pathways and that effective stress is only locally altered.

We have proposed a four stage interpretation to gas flow through COx that suggests that gas migration is the result of dilatant gas pathway formation. The response of COx during the onset of gas flow is very complex and the current report has highlighted a number of uncertainties that require careful modelling in order to fully decouple the effects of swelling as a result of water expulsion from the injection guard ring, the mechanical response to changes in effective stress and the migration of gas along dilatant gas pathways. It is recommended that a suitable modelling team be approached in order to determine fully the underlying physics of the gas flow through COx. The observations reported here strengthen the argument for dilatant pathway propagation.



Time	Injection flow	Injection guard	Back pressure guard	Load cell	Radial strain 1	Radial strain 2	Radial strain 3	Axial strain	Back pressure flow	Related to temperature	Pump status	Time interval	Time interval (gas)	
205.75				∧	#	#	#			Y	Constant flow mode			
208.35				∨										
211.6				∧										
216				#										
218.5					#	#	#							
220				#										
220.45				#										
221.875	#			↓										0.0
222.25					#	#	#			?				0.4
223.5				∧										1.6
232.85		#	#					Blip		?				11.0
233				#										11.1
233.95				#										12.1
235.25							#			?				13.4
235.87		#	#							?				14.0
236.2					#	↓				?				14.3
236.5				#min		∨	#			∧				14.6
237.32				↑										15.4
237.57				∧										15.7
238.55		Gas		#										16.7
239.8					#	#_	#							17.9
240.5			#											18.6
241.85			#	↓										20.0
242.2									#					20.3
243.5						#↓	#_							21.6
245.5					#	∨								23.6
246.45						∧	∧							24.6
247.5									#					25.6
250					∧								28.1	
251.5					#		#						29.6	
254						↓↓						0	32.1	
254.5									#			0.5	32.6	
254.7037		↑			↓↓			#				0.7	32.8	
255.03											Constant pressure mode	1.0	33.2	
255.13		∧					↓↓					1.1	33.3	
255.6			#						#			1.6	33.7	
256.5				#								2.5	34.6	
257									#			3	35.1	
262				∧					#			8	40.1	
265.03								↑				11.0	43.2	
269.5									#_					47.6
271.1				↑										49.2
273			# Gas											51.1
273.105			∨											51.2
273.4			#											51.5
273.9			#											52.0
274.05			∨											52.2
274.3			#											52.4
274.9			↓										53.0	

**Table 9-4** Summary of all events relevant to onset of gas flow through the COx. Key: # = deflection in reading; #\_ = reading has reached plateau; ↑ = sharp increase in reading; ↓ sharp decrease in reading; ↓↓ = onset of accelerated radial strain; ∧ = peak in reading; ∨ = trough in reading; Gas = evidence that gas has reached guardrings.

## References

British Geological Survey holds most of the references listed below, and copies may be obtained via the library service subject to copyright legislation (contact libuser@bgs.ac.uk for details). The library catalogue is available at: <http://geolib.bgs.ac.uk>.

- Cuss, R.J. and Harrington, J.F. (2010) Effect of stress field and mechanical deformation on permeability and fracture self-sealing: Progress Report on the Stress Path Permeameter experiment conducted on Callovo-Oxfordian claystone. British Geological Survey Commissioned Report, CR/10/151. 71pp.
- Esteban, L., Bouchez, J., L. and Trouiller, A. (2006) The Callovo-Oxfordian argillites from the eastern Paris Basin: Magnetic data and petrofabrics, *Comptes Rendus Geosciences* **338**, pp 867-881
- Gaucher, E., Robelin, C., Matray, J.-M., Négrel, G., Gros, Y., Heitz, J.-F., Vinsot, A., Rebours, H., Cassagnabère, A. and Bouche, A.T. (2004) ANDRA underground research laboratory: interpretation of the mineralogical and geochemical data acquired in the Callovo-Oxfordian formation by investigative drilling, *Phys. Chem. Earth* **29**, pp. 55–77.
- Horseman, S.T., Harrington, J.F., Birchall, D.J., Noy, D.J. and Cuss, R.J. (2005). Consolidation and rebound properties of Opalinus clay: A long-term, fully-drained test. *British Geological Survey Commissioned Report*. **CR/05/128**. 60 pp (Commercial - In Confidence).
- Rouseset, D. and Clauer, N. (2003) Discrete Clay Diagenesis in a Very Low-Permeable Sequence Constrained by an Isotopic (K-Ar and Rb-Sr) Study, *Contributions to Mineralogy and Petrology*, **145**, pp 182-198.
- Wenk, H.-R., Voltolini, M., Mazurek, M., Van Loon, L.R. and Vinsot, A. (2008) Preferred Orientations and Anisotropy in Shales: Callovo-Oxfordian Shale (France) and Opalinus Caly (Switzerland), *Clays and Clay Minerals*, **56**, pp 285-306.
- Wileveau, Y., and Bernier, F. (2008) Similarities in the hydromechanical response of Callovo-Oxfordian clay and Boom Clay during gallery excavation. *Physics and Chemistry of the Earth*, **33**, S343–S349.
- Zhang, C-L, Rothfuchs, T., Su, K., and Hoteit, N. (2007) Experimental study of the thermo-hydro-mechanical behaviour of indurated clays. *Physics and Chemistry of the Earth*, **32**, 957–965.